ACS OMEGA

http://pubs.acs.org/journal/acsodf

Article

Delicate Design of ZnS@In_2S_3 Core–Shell Structures with Modulated Photocatalytic Performance under Simulated Sunlight Irradiation

Jianyi Lu, Qianqian Guo, Jingyang Chen, Kunhan Xie, Xiaohui Guan,* Liu Yang,* and Guangsheng Wang*

Cite This: *ACS Omega* 2023, 8, 529–538

Read Online

ACCESS | Metrics & More | Article Recommendations | Supporting Information

ABSTRACT: ZnS@In_2S_3 core–shell structures with high photocatalytic activity have been delicately designed and synthesized. The unique structure and synergistic effects of the composites have an important influence on the improvement of photocatalytic activity. The photocatalytic activity has been studied by photodegrading individual eosin B (EB) and the mixture solution consisting of eosin B and rhodamine B (EB-RhB) in the presence of hydrogen peroxide (H_2O_2) under simulated sunlight irradiation. The results show that all of the photocatalysts with different contents of In_2S_3 exhibit enhanced catalytic activity compared to pure ZnS for the degradation of EB and EB-RhB solution. When the theoretical molar ratio of ZnS to In_2S_3 was 1:0.5, the composite presents the highest photocatalytic efficiency, which could eliminate more than 98% of EB and 94% of EB-RhB. At the same time, after five cycles of photocatalytic tests, the photocatalytic efficiency could be about 96% for the degradation of the EB solution, and relatively high photocatalytic activity could also be obtained for the degradation of the EB-RhB mixed solution. This work has proposed a facile synthetic process to realize the controlled preparation of core–shell ZnS@In_2S_3 composites with effectively modulated structures and compositions, and the composites have also proved to be high-efficiency photocatalysts for the disposal of complicated pollutants.

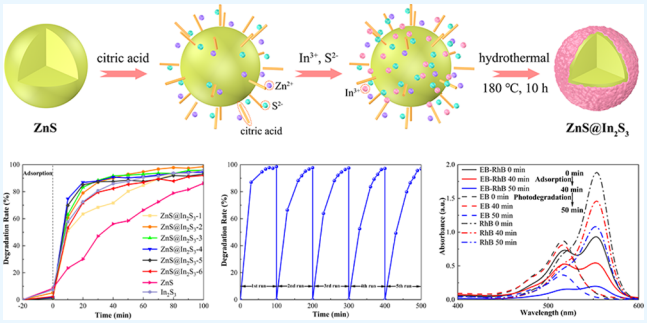

1. INTRODUCTION

Photocatalysis has been considered to be a highly efficient and economic method to dispose of organic pollutants in water and has attracted increasing attention recently.[1−4] Among the various kinds of photocatalysts, metal chalcogenides have been widely studied, such as ZnS,[5−8] Bi_2S_3,[9−11] CuS,[12−14] CdS,[15−17] and so on, because of their controllable band structures and excellent performance for photocatalytic degradation of organic pollutants under light irradiation. However, some shortcomings, such as low solar utilization efficiency, toxicity, and rapid recombination of photogenerated electron–hole pairs, prevent their extensive applications.[18−21] The reported research studies indicate that the design and synthesis of chalcogenide composites is an effective method to improve the photocatalytic performance in the degradation process.[22−26]

ZnS is a well-known ultraviolet light-driven photocatalyst, which has been extensively studied due to its relatively high photocatalytic activity.[7,15,27,28] Although ZnS is a wide-band-gap semiconductor (3.72 eV for the cubic crystalline, 3.77 eV for the hexagonal crystalline), its photocatalytic activity could be effectively improved. Based on the previous reports, the following methods could dramatically enhance its photocatalytic performance. Modulating the morphology and structure of ZnS nanomaterials would be an efficient way to increase the active sites and regulate the migration of photoinduced charge carriers.[29−31] Furthermore, the photocatalytic efficiency could be noticeably enhanced by adjusting the band gap of the photocatalysts, which could optimize their activity and light utilization efficiency during the degrading process.[32−34] Many researchers have made efforts to improve the photocatalytic activity of ZnS. Das et al.[35] prepared a kind of CuS/ZnS (CZS) nanoparticles (NPs) that grew on graphene sheets through a simple and green synthesis. By comparison, the visible light photocatalytic activity of CuS/ZnS graphene (CZSG) nanocomposites for the degradation of methylene blue was significantly enhanced. Ouni et al.[36] synthesized thioglycolic acid-decorated ZnS nanocrystals and tested the photodegradation efficiency for methyl orange aqueous solution. The results showed that the dye pollutant could be degraded for 81.37% after 6 min. Kumar[37] prepared ZnS nanoparticles with poly(ethylene glycol)-4000 (PEG-

Received: August 25, 2022
Accepted: December 5, 2022
Published: December 28, 2022

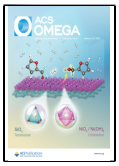

https://doi.org/10.1021/acsomega.2c05483
ACS Omega 2023, 8, 529–538

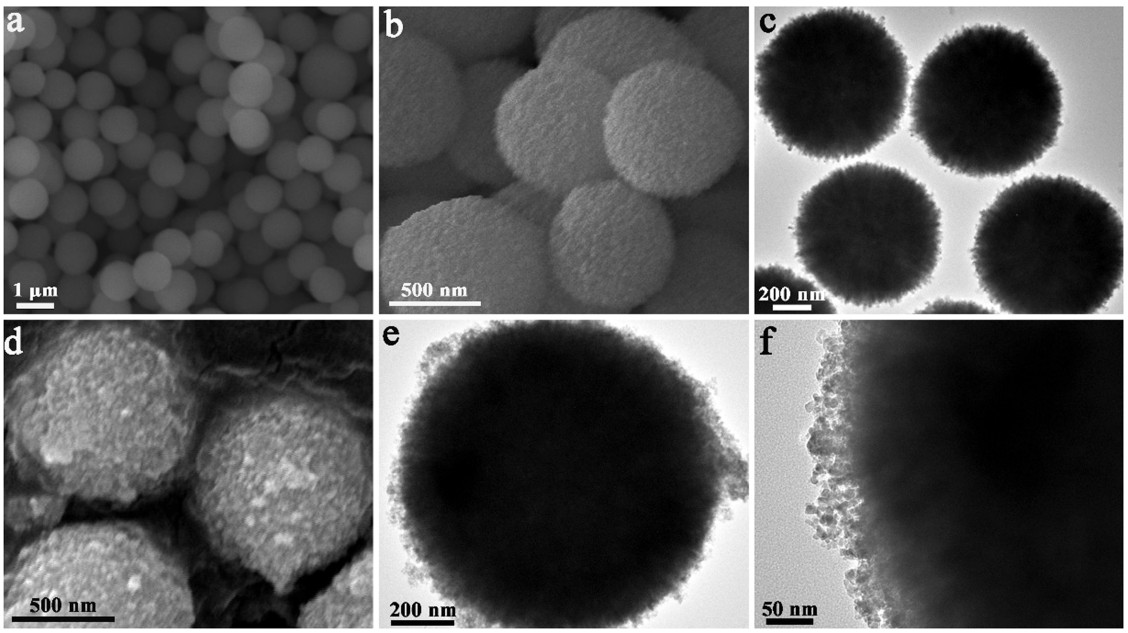

Figure 1. (a, b) SEM and (c) TEM images of ZnS. (d) SEM and (e, f) TEM images of ZnS@In_2S_3-2.

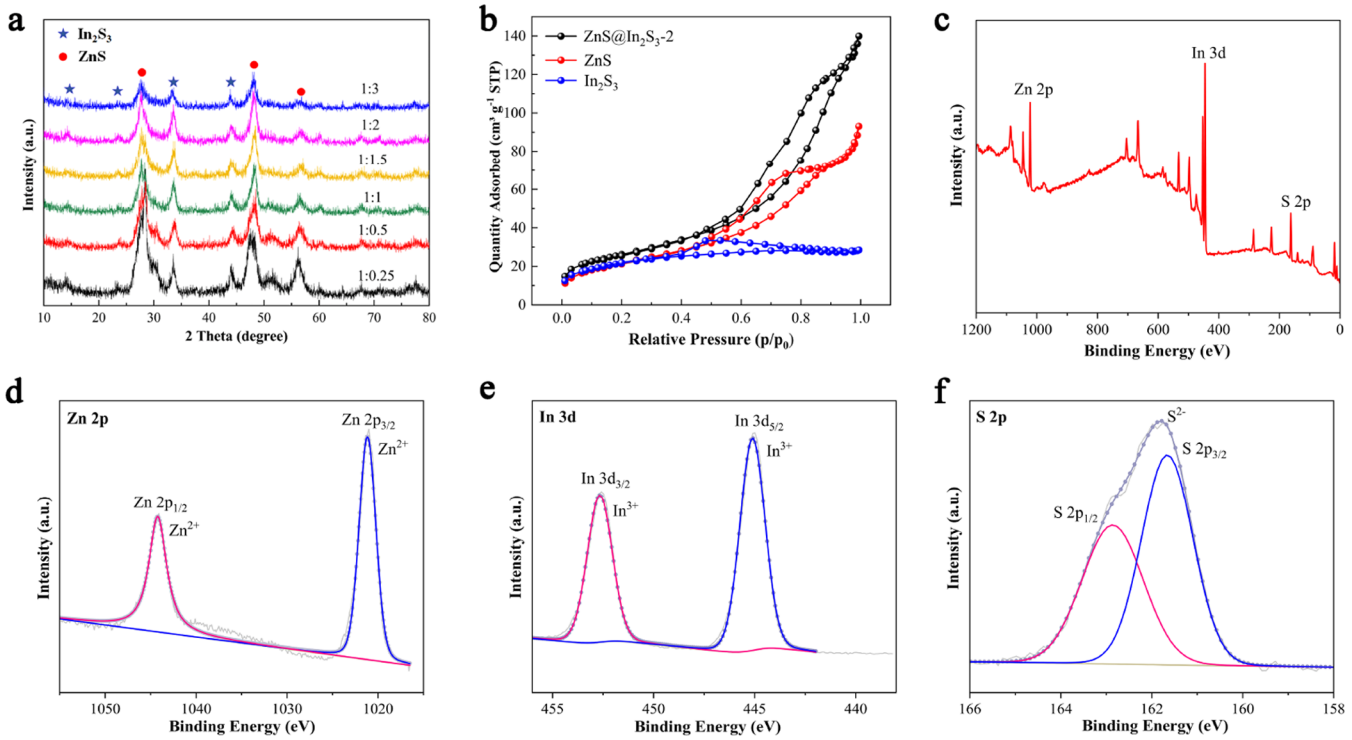

Figure 2. (a) XRD patterns of the ZnS@In_2S_3 composites. (b) N_2 adsorption−desorption isotherm loops of ZnS, In_2S_3, and ZnS@In_2S_3-2. XPS spectra of ZnS@In_2S_3-2: (c) survey spectrum, (d) Zn 2p spectrum, (e) In 3d spectrum, and (f) S 2p spectrum.

4000) or poly(vinylpyrrolidone) (PVP) capping by chemical precipitation. The photocatalytic degradation test of the solution containing methyl orange dye showed that the photocatalytic degradation rate of PEG-ZnS reached 85%, and the photocatalytic degradation rate of PVP-ZnS was 87%, which was obviously better than that of untreated ZnS. However, the reported research studies generally focus on the disposal of pollutants containing a single dye, which greatly limits their applications in practical wastewater treatment. Thus, it is of great significance to explore high-efficiency photocatalysts for more complicated water pollutants.

In this work, a facile synthetic process has been proposed for the controlled preparation of core−shell structure ZnS@In_2S_3 composites, which present high solar light utilization efficiency and photocatalytic activity. Additionally, the photocatalytic performance for the degradation of single and mixed dye solutions has also been investigated. The experimental results show that the unique structure and composition have a remarkable influence on the photocatalytic efficiency of the

https://doi.org/10.1021/acsomega.2c05483
ACS Omega 2023, 8, 529−538

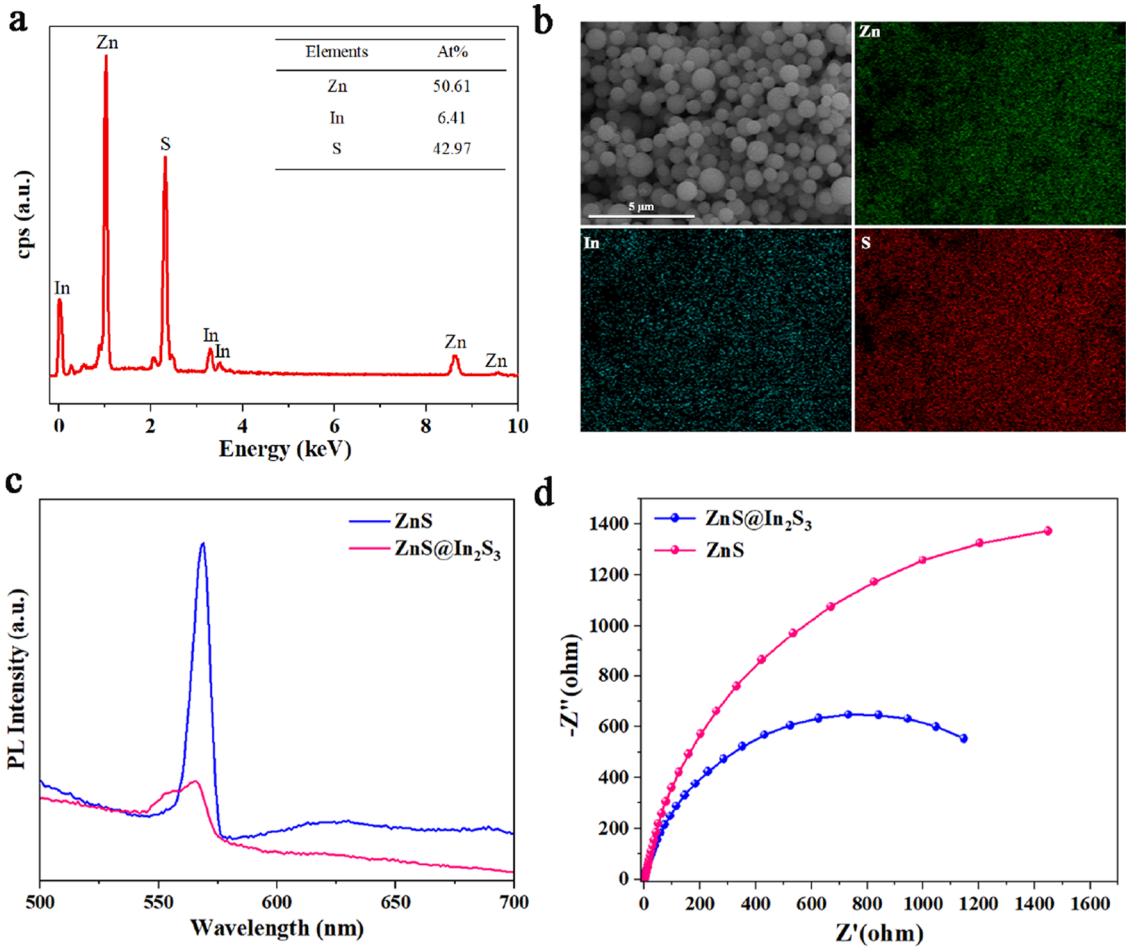

Figure 3. (a, b) EDX analysis of ZnS@In_2S_3-2. (c) PL and (d) EIS results of ZnS and ZnS@In_2S_3-2.

synthesized photocatalyst. ZnS@In_2S_3-2 exhibits a high degradation efficiency of 98.55% for pure EB solution and over 94% degradation efficiency for the EB-RhB mixed solution. This study has provided a novel and feasible way to modulate the performance of photocatalysts for practical applications.

2. RESULTS AND DISCUSSION

2.1. Characterization of the Photocatalyst. The morphology and structure of the prepared ZnS and ZnS@In_2S_3-2 composite are analyzed by field emission scanning electron microscopy (FESEM) and transmission electron microscopy (TEM). Figure 1a,b shows that ZnS presents a uniform sphere structure with an average diameter of about 800 nm, and the surface of the spheres is slightly rough. From Figure 1c, it is clear that the surface of ZnS spheres is not smooth, which is beneficial for the decoration of In_2S_3 nanoparticles. Moreover, the spheres have a solid structure, which is conducive to the retention of photocatalytic efficiency during the cyclic utilization process. Figure 1d−f shows that the surface of the ZnS@In_2S_3-2 sphere structures becomes rougher, and numerous In_2S_3 nanoparticles are uniformly decorated on the surface, forming a unique core−shell structure.

The crystalline structure and composition of the as-prepared ZnS@In_2S_3 composites are confirmed by X-ray diffraction (XRD) analysis. As shown in Figure 2a, all of the materials show evident diffraction peaks for ZnS (JCPDS No. 75-1547) and In_2S_3 (JCPDS No. 84-1385). The XRD pattern for pure ZnS is shown in Figure S1, and the crystalline structures are the same as those of the composites. The results indicate that all of the ZnS@In_2S_3 composites are composed of ZnS and In_2S_3, and as the coating amount of In_2S_3 is increased gradually, several diffraction peaks for ZnS become weaker and inconspicuous, which demonstrates that In_2S_3 is coated outside the ZnS sphere.

The specific surface areas of ZnS, In_2S_3, and ZnS@In_2S_3 composites are investigated, and the results are displayed in Figure 2b and Table S1. It could be observed that the ZnS@In_2S_3 composites exhibit higher specific surface areas than bare ZnS (78.3 $m^2\ g^{-1}$) and In_2S_3 (73.8 $m^2\ g^{-1}$), which could provide much more active sites for the photocatalytic degradation of organic dyes. When the theoretical molar ratio of ZnS to In_2S_3 increases to 1:1.5, the composite exhibits the highest specific surface area of 136.7 $m^2\ g^{-1}$. However, when the content of In_2S_3 is continually increased, the specific surface area decreases a little because of the obvious aggregation of the nanostructures resulting from a large amount of In_2S_3 nanoparticles. The results demonstrate that the introduction of a moderate amount of In_2S_3 could effectively improve the contact area for both adsorption and photocatalytic degradation of dye molecules.

The surface elemental composition and chemical state of the ZnS@In_2S_3-2 composite are investigated by X-ray photoelectron spectroscopy (XPS). As shown in Figure 2c, the survey spectrum indicates that the ZnS@In_2S_3-2 composite

https://doi.org/10.1021/acsomega.2c05483
ACS Omega 2023, 8, 529−538

Scheme 1. Schematic Description for the Synthesis of ZnS@In_2S_3 Core−Shell Structures

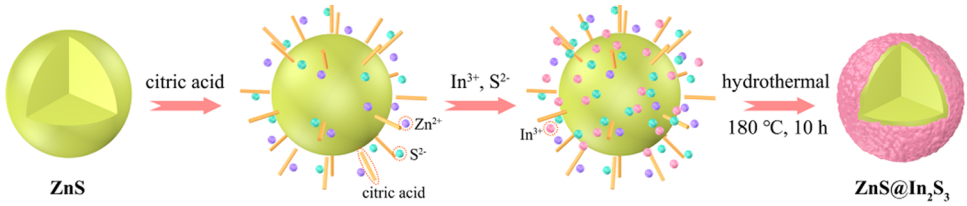

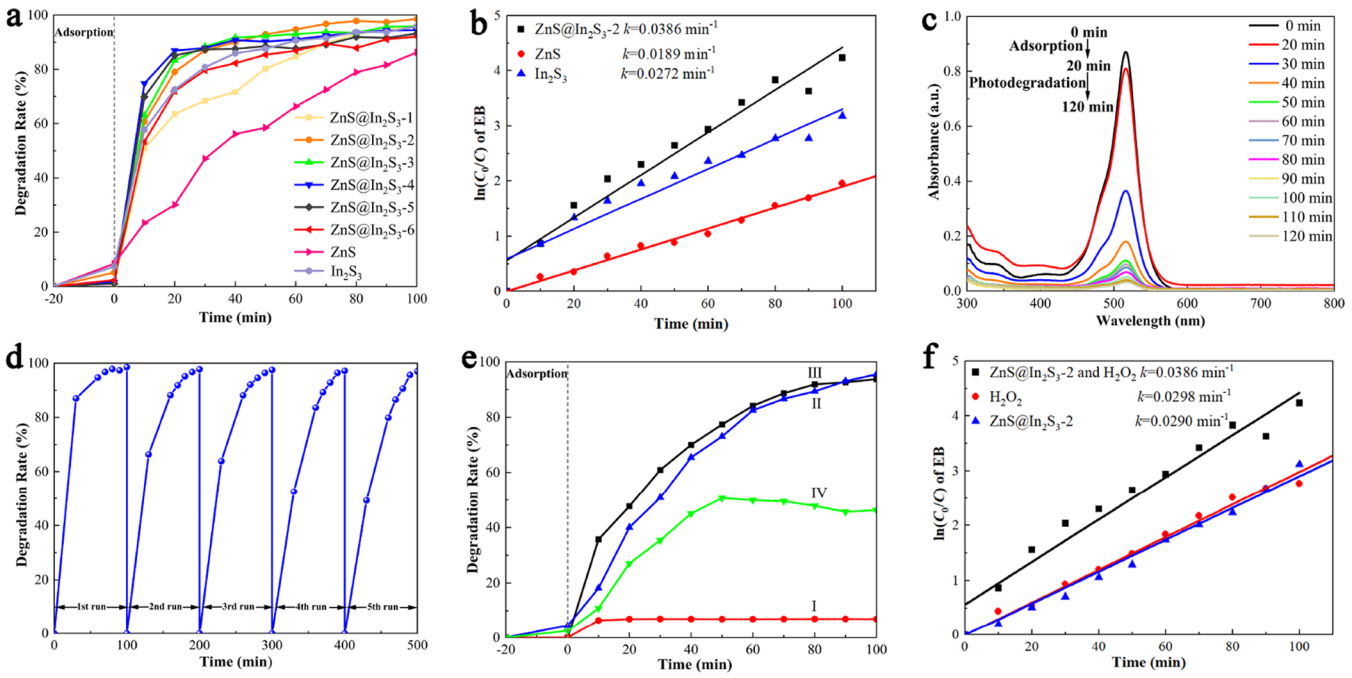

Figure 4. (a) Photocatalytic efficiencies of ZnS, In_2S_3, and ZnS@In_2S_3 composites. (b) Plots of $\ln(C_0/C)$ as a function of simulated sunlight irradiation time for the degradation of EB with the photocatalysts of ZnS, In_2S_3, and ZnS@In_2S_3-2. (c) The real-time UV−vis absorption spectra of EB during the photocatalytic degradation process with the photocatalyst of ZnS@In_2S_3-2. (d) Cycle performance of ZnS@In_2S_3-2. (e) Elimination rates of EB by ZnS@In_2S_3-2 in the dark (I), by ZnS@In_2S_3-2 under simulated sunlight (II), by H_2O_2 under simulated sunlight (III), and by ZnS@In_2S_3-2 and H_2O_2 in the dark (IV). (f) Plots of $\ln(C_0/C)$ as a function of simulated sunlight irradiation time for the degradation of EB with ZnS@In_2S_3-2 and H_2O_2, H_2O_2, and ZnS@In_2S_3-2.

consists of Zn, S, and In elements. In Figure 2d, the Zn 2p spectrum could be divided into two peaks, Zn $2p_{1/2}$ and Zn $2p_{3/2}$, centered at 1044.1 and 1021 eV, respectively, which correspond to Zn^{2+}.[33−35] In Figure 2e, the characteristic peaks at 444.9 and 452.6 eV could be assigned to In $3d_{5/2}$ and In $3d_{3/2}$, respectively, indicating that the In element exists in the +3 valance state.[36] In Figure 2f, S 2p could be fitted into S $2p_{1/2}$ and S $2p_{3/2}$, which represent the S element in the −2 valence state.[37] The XPS results have further affirmed the composition of the material, which is consistent with the previous analysis.

Energy-dispersive X-ray spectroscopy (EDX) analysis has been adopted to confirm the contents and distributions of the Zn, In, and S elements in the ZnS@In_2S_3-2 composite, and the results are shown in Figure 3a,b. As can be seen, ZnS@In_2S_3-2 is composed of Zn, In, and S elements, which are uniformly distributed in the nanomaterial. Moreover, it is clear that the content of ZnS in the composite is much higher than that of In_2S_3, which is consistent with the TEM results, and the small amount of In_2S_3 has been proven to be able to dramatically improve the photocatalytic performance of the composite. The PL and EIS analyses have been applied to confirm the dynamic behavior of the photoexcited carriers of ZnS and the ZnS@In_2S_3-2 composite. As can be seen in Figure 3c, the PL emission peak intensity of ZnS@In_2S_3-2 is much lower than that of ZnS, which completely demonstrates that the coating of a thin layer of In_2S_3 could effectively improve the separation and migration efficiency of the photoinduced carriers.[31,38] Moreover, in Figure 3d, the relatively smaller arc of ZnS@In_2S_3-2 indicates its better charge diffusion ability than individual ZnS.[8,39] The PL and EIS results have revealed that the synergistic effects between ZnS and In_2S_3 could noticeably optimize the dynamic behavior of the photocatalyst.

The synthesis mechanism of ZnS@In_2S_3 composites is analyzed and described, as shown in Scheme 1. ZnS spheres are utilized as the precursor, and the In_2S_3 nanoparticles could grow outside the ZnS surface via the ion exchange and deposition process. First, ZnS spheres are able to release few Zn^{2+} and S^{2-} ions in the citric acid solution and form a dynamic balance. Citrate acid also plays a role as a functional agent to induce the In^{3+} ions to react with S^{2-} ions on the surface of ZnS. The solubility product constant for ZnS (2.93×10^{-22}) is much larger than that of In_2S_3 (5.7×10^{-74}), indicating that the In^{3+} ions tend to exchange Zn^{2+} in ZnS during the reaction. When the In^{3+} ions are added to the ZnS aqueous dispersion, the original chemical equilibrium would be

https://doi.org/10.1021/acsomega.2c05483
ACS Omega 2023, 8, 529−538

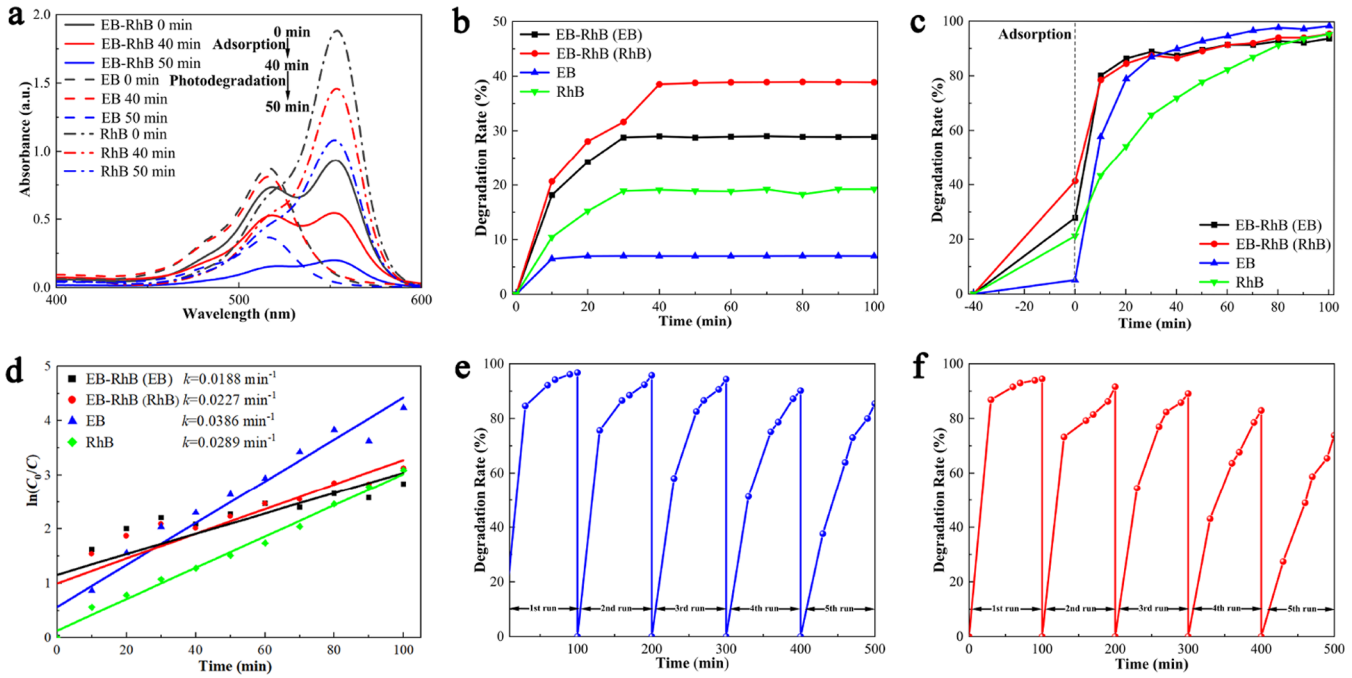

Figure 5. (a) UV−vis absorption spectra of EB-RhB, EB, and RhB during the photocatalytic degradation process. (b) Elimination rates of EB-RhB, EB, and RhB with ZnS@In_2S_3-2 in the dark. (c) Degradation rates of EB-RhB, EB, and RhB with ZnS@In_2S_3-2 and H_2O_2 under simulated sunlight irradiation. (d) Plots of $\ln(C_0/C)$ as a function of simulated sunlight irradiation time for the degradation of EB-RhB, EB, and RhB with ZnS@In_2S_3-2. (e, f) Repetitive utilization of ZnS@In_2S_3-2 in EB-RhB solution for the degradation of RhB and EB.

broken, and the ion exchange reaction occurs. In^{3+} ions could combine with S^{2-} ions to form In_2S_3, and the product would load on the surface of ZnS. As the surface of ZnS is evenly coated with In_2S_3, it could prevent In^{3+} ions from further exchanging Zn^{2+} in ZnS; thus, a new chemical equilibrium could be established. Furthermore, during the solvothermal process, extra added S^{2-} ions could rapidly react with In^{3+} ions. Because the surface of ZnS spheres has already been coated by In_2S_3 nanoparticles, the newly generated ones are more likely to continually grow on the sphere structures and form a thicker In_2S_3 shell. The corresponding reactions could be proposed as follows

$$ZnS \leftrightarrow Zn^{2+} + S^{2-} \quad (1)$$

$$2In^{3+} + 3S^{2-} \leftrightarrow In_2S_3 \quad (2)$$

$$3ZnS + 2In^{3+} \leftrightarrow In_2S_3 + 3Zn^{2+} \quad (3)$$

2.2. Photocatalytic Performance. The optical property of ZnS@In_2S_3-2 is assessed and shown in Figure S2. It could be found that via the combination of In_2S_3, the light absorption range has been widened, which could utilize the light over the wavelength of 400 nm. The photocatalytic performance of the ZnS@In_2S_3 composites for the degradation of EB is compared with that of bare ZnS spheres and In_2S_3 nanoparticles. As shown in Figure 4a, in the first 20 min, it is mainly the adsorption process of the photocatalysts for dye molecules in the presence of H_2O_2 without light irradiation. The EB molecules could absorb on the photocatalysts and reach the adsorption−desorption equilibrium. Evidently, the adsorption rates of the ZnS@In_2S_3 composites are below 10%, indicating that the removal of organic pollutants is mainly attributed to the photocatalytic process. After being exposed to light irradiation for 100 min, the removal rates of EB are 95.68, 98.55, 95.90, 94.42, 93.19, and 92.06% for ZnS@In_2S_3-1, ZnS@In_2S_3-2, ZnS@In_2S_3-3, ZnS@In_2S_3-4, ZnS@In_2S_3-5, and ZnS@In_2S_3-6, respectively. For bare ZnS, the EB removal efficiency could hardly reach 90% in 100 min, and for bare In_2S_3 nanoparticles, the degradation rate is up to 95.83%. The results indicate that the In_2S_3 nanoparticles present much higher photocatalytic efficiency than ZnS spheres, and the appropriate combination of In_2S_3 in the composites could improve the photocatalytic performance owing to the synergistic effects. When the theoretical molar ratio of ZnS to In_2S_3 is 1:0.5, the composite presents the highest photocatalytic efficiency. Moreover, the elimination rate of TOC utilizing ZnS@In_2S_3-2 as the photocatalyst is also investigated, and 50.7% of the TOC could be eliminated during the photocatalytic process.

The kinetics of EB degradation during the photocatalytic process is also analyzed. As shown in Figure 4b, linear relationships between $\ln(C_0/C)$ and reaction time are obtained, indicating that the photocatalytic degradation of EB follows the first-order kinetics. The apparent rate constants are calculated to be 1.899×10^{-2}, 2.72×10^{-2}, and 3.86×10^{-2} min^{-1} for ZnS, In_2S_3, and ZnS@In_2S_3-2, respectively, which demonstrates that the ZnS@In_2S_3-2 composite exhibits a higher degradation rate for the pollutants. The real-time ultraviolet−visible (UV−vis) absorption spectra of the EB solution during the photocatalytic process with the ZnS@In_2S_3-2 photocatalyst are shown in Figure 4c. It could be observed that the intensity of the characteristic peak of EB at 514 nm decreases gradually. In the first 20 min, the intensity of the characteristic peak decreases slightly, due to the relatively weak adsorption ability of ZnS@In_2S_3-2. After exposure to light irradiation for 100 min, the intensity of the peak obviously decreases, which proves that EB is successfully degraded in the presence of ZnS@In_2S_3-2 and H_2O_2 under light irradiation. During the whole photocatalytic degradation

https://doi.org/10.1021/acsomega.2c05483
ACS Omega 2023, 8, 529−538

Scheme 2. Mechanism for the Photocatalytic Degradation of Dye Pollutants by the ZnS@In_2S_3 Composite

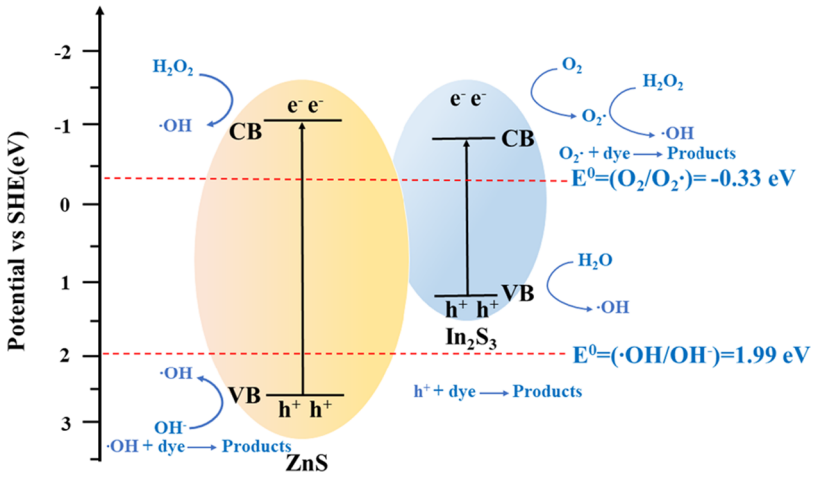

process, none of the extra peaks are formed, which might demonstrate that there are no complicated organic impurities generated. The cycle performance of ZnS@In_2S_3-2 as a photocatalyst is also assessed, and the results are shown in Figure 4d. After repetitive utilization for 5 cycles, there is no significant loss in the photocatalytic efficiency for the degradation of EB, which suggests that the ZnS@In_2S_3-2 composite exhibits ideal cycle performance and has the potential for practical applications.

The results of the blank experiments are displayed in Figure 4e. According to the ZnS@In_2S_3-2 adsorption experiment performed in the dark (curve I), ZnS@In_2S_3-2 reaches the adsorption−desorption equilibrium within 20 min for the adsorption of EB molecules. In addition, the degradation rate of EB with the presence of ZnS@In_2S_3-2 under light irradiation is as high as over 90% (curve II), which indicates that ZnS@In_2S_3-2 possesses excellent photocatalytic performance for the removal of organic dyes. Moreover, utilizing H_2O_2 individually could achieve a relatively great degradation effect for EB under light irradiation in 100 min (curve III). On the contrary, about 46.23% of EB could be eliminated with the presence of ZnS@In_2S_3-2 and H_2O_2 in the dark, which is much lower than that performed under the simulated sunlight (curve IV). According to Figure 4f, the apparent rate constants for the degradation of EB with the presence of ZnS@In_2S_3-2 and H_2O_2, ZnS@In_2S_3-2, and H_2O_2 are 3.86×10^{-2}, 2.90×10^{-21}, and 2.98×10^{-2} min^{-1}, respectively. It is obvious that although the degradation rate is relatively high when H_2O_2 is added individually, the reaction rate is slower than the photocatalytic degradation process. The results have indicated that ZnS@In_2S_3-2 possesses high photocatalytic performance.

The photocatalytic performance of ZnS@In_2S_3-2 has been further evaluated via degradation of the mixed dye solution composed of EB and RhB (EB-RhB). As shown in Figure 5a, the real-time concentrations of EB-RhB, EB, and RhB solutions are measured by UV−vis absorption spectroscopy. The intensity of the characteristic absorption peak of EB at 514 nm and the peak of RhB at 552 nm for the mixed dye solution and the single dye solution are quite weak after the photocatalytic degradation process. According to Figure 5b, it is clear that the absorption−desorption equilibrium could be established after 20, 30, and 40 min for the EB solution, RhB solution, and EB-RhB solution, respectively. As shown in Figure 5c, the photocatalytic degradation efficiency for EB could reach 94.5% in the EB-RhB mixed solution after light irradiation for 100 min, which is slightly lower than that in the individual EB solution. In contrast, the degradation rate for RhB is relatively higher in the EB-RhB solution than that in the individual RhB solution. The kinetics of photocatalytic degradation of EB-RhB, EB, and RhB is shown in Figure 5d. It could be observed that the apparent rate constants have a small difference, which indicates that utilizing ZnS@In_2S_3-2 as the photocatalyst could achieve high efficiency and degradation rate in both the individual and dual dye pollutant systems. The photocatalytic stability of ZnS@In_2S_3-2 for the disposal of the EB-RhB solution is also evaluated, and the results are shown in Figure 5e,f. The degradation efficiencies for EB and RhB decrease gradually and could maintain 73.83 and 85.42% in the EB-RhB solution after repetitive utilization for five cycles. The decreased photocatalytic degradation efficiency might be mainly attributed to the mass loss during the recycling process. The ion leaching from the ZnS@In_2S_3-2 photocatalyst during the degradation process has been studied using the EDX characterization, and the results are shown in Figure S3. It could be found that the Zn, In, and S elements distribute uniformly in the nanostructures after the photocatalytic process for the degradation of EB or EB-RhB, which indicates that the as-prepared photocatalysts exhibit great stability during the degradation process. Moreover, after utilization for the elimination of EB and EB-RhB, the content of the Zn element in the composite reduces, indicating the Zn^{2+} ions leaching, and this might be one of the reasons for the performance decrease of the photocatalyst during the repetitive utilization process.

The mechanism for the photocatalytic degradation of EB and RhB has been investigated and shown in Scheme 2. First, the heterostructures of the ZnS@In_2S_3 composites are combined with a wide-band-gap material and a narrow-band-gap material, which could effectively improve the light utilization efficiency and facilitate the separation of the photoexcited electron−hole pairs.[40,41] During the photocatalytic degradation process, the semiconductors could absorb the optical energy and generate photoexcited electrons and holes in the conduction band (CB) and the valence band (VB), respectively (eq 4).[42,43] The photoinduced holes existing in the VB could directly oxidize organic molecules into nontoxic products. Moreover, they are also able to react with H_2O to produce $^{\bullet}OH$ radicals (eqs 5 and 6). Additionally, the

https://doi.org/10.1021/acsomega.2c05483
ACS Omega 2023, 8, 529−538

oxidizing agents, H_2O_2 and O_2, dissolved in the solution could scavenge the photogenerated electrons to form $^{\bullet}OH$ and $^{\bullet}O_2^-$ radicals, respectively. Generally, $^{\bullet}O_2^-$ radicals are also capable of reacting with H_2O_2 to produce more $^{\bullet}OH$ radicals (eqs 7, 8, and 9). The two kinds of radicals could effectively degrade the dye pollutants into inorganic and nontoxic products (eqs 10 and 11). As extra H_2O_2 is added in this work, $^{\bullet}OH$ radicals are considered to play the main role in the degradation of EB and RhB pollutants. The possible mechanism for the photocatalytic degradation of dye molecules could be proposed as follows:[44,45]

$$ZnS@In_2S_3 + h\nu \rightarrow h^+ + e^- \quad (4)$$

$$h^+ + \text{dye} \rightarrow \text{products} \quad (5)$$

$$h^+ + H_2O \rightarrow {}^{\cdot}OH + H^+ \quad (6)$$

$$H_2O_2 + e^- \rightarrow {}^{\cdot}OH + OH^- \quad (7)$$

$$O_2 + e^- \rightarrow {}^{\cdot}O_2^- \quad (8)$$

$$^{\cdot}O_2^- + H_2O_2 \rightarrow OH^- + O_2 + {}^{\cdot}OH \quad (9)$$

$$^{\cdot}O_2^- + \text{dye} \rightarrow \text{products} \quad (10)$$

$$^{\cdot}OH + \text{dye} \rightarrow \text{products} \quad (11)$$

3. CONCLUSIONS

In summary, $ZnS@In_2S_3$ core−shell structures have been successfully fabricated via a delicately designed process. The unique heterostructures and the synergistic effects between the composites have effectively optimized the charge transfer behavior and the photocatalytic activity. The photocatalytic degradation efficiency for EB could reach 98.55%, and after five repetitive cycles, the efficiency nearly has no loss. In addition, the as-prepared $ZnS@In_2S_3$-2 composite also possesses ideal photocatalytic performance for the degradation of EB-RhB mixed pollution, and the degradation efficiency is over 94%. This study has provided a facile method for the controlled synthesis of high-performance photocatalysts as well as their performance modulation, and the $ZnS@In_2S_3$ core−shell structures prepared here have proved to be of great potential for the disposal of organic pollutants.

4. EXPERIMENTAL SECTION

4.1. Materials. All of the reagents were of analytical grade and used without further purification. The water used in this work was ultrapure water.

4.2. Synthesis of the Photocatalyst. *4.2.1. Preparation of ZnS Spheres.* ZnS spheres were synthesized by a facile solvothermal method. In a typical procedure, 3 mmol of $Zn(Ac)_2{\cdot}2H_2O$ and 6 mmol of L-cysteine were dissolved in the mixed solution of 10 mL of glycerin, 20 mL of triethanolamine, and 38 mL of ultrapure water. Then, the mixture was stirred for 10 min, and the basicity of the solution was adjusted by adding 12 mL of ammonia water. Afterward, the homogeneous solution was transferred into a 100 mL Teflon-lined stainless steel autoclave and heated at 170 °C for 16 h. After air cooling to room temperature, the white product was collected by centrifugation, washed with ultrapure water and ethanol several times to eliminate the impurities, and finally dried in a vacuum oven at 60 °C for 24 h.

4.2.2. Preparation of $ZnS@In_2S_3$ Core−Shell Structures. First, 0.56 mmol of the ZnS precursor was uniformly dispersed in 40 mL of ultrapure water containing 0.16 mmol of citric acid, and the solution was stirred continuously in a 60 °C water bath for 2 h and then cooled down to room temperature. Afterward, 20 mL of ultrapure water containing 0.28 mmol of $In(NO_3)_3{\cdot}4.5H_2O$ was slowly added to the above ZnS dispersion and stirred magnetically for 2 h at room temperature. Subsequently, 20 mL of ultrapure water containing 0.56 mmol of $Na_2S{\cdot}9H_2O$ was added dropwise, and the mixed solution was stirred at room temperature for another 1 h. Finally, the above solution was transferred to a 100 mL Teflon-lined stainless steel autoclave and heated at 180 °C for 10 h. The forming precipitate was centrifuged and washed with ultrapure water and ethanol several times and then dried in a vacuum oven at 60 °C for 24 h to obtain the $ZnS@In_2S_3$ core−shell structures. To optimize the photocatalytic efficiency of the products, the ratio of the coated In_2S_3 was regulated. ZnS was fixed at 0.56 mmol, and the theoretical molar ratio of ZnS to In_2S_3 was adjusted to 1:0.25, 1:0.5, 1:1, 1:1.5, 1:2, and 1:3. The corresponding products were named $ZnS@In_2S_3$-1, $ZnS@In_2S_3$-2, $ZnS@In_2S_3$-3, $ZnS@In_2S_3$-4, $ZnS@In_2S_3$-5, and $ZnS@In_2S_3$-6, respectively.

4.2.3. Preparation of In_2S_3 Nanoparticles. To further investigate the effects of the composition and structure on the photocatalytic activity of the $ZnS@In_2S_3$ composites, pure In_2S_3 was also synthesized according to the previous report.[46] First, 0.56 mmol of $In(NO_3)_3{\cdot}4.5H_2O$ and 1.12 mmol of $Na_2S{\cdot}9H_2O$ were separately dissolved in 40 mL of ultrapure water.[47,48] Then, $Na_2S{\cdot}9H_2O$ solution was added gradually into the $In(NO_3)_3{\cdot}4.5H_2O$ solution under stirring for 1 h, and the mixed solution was loaded in a 100 mL Teflon-lined autoclave and heated at 180 °C for 16 h. After air cooling to room temperature, the In_2S_3 nanoparticles were washed with ultrapure water and ethanol several times and finally dried in a vacuum oven at 60 °C.

4.3. Characterization. The crystalline structure of the products was confirmed by the X-ray diffraction (XRD) characterization conducted on an X-ray powder diffractometer (Philips X'pert Pro Super) with Cu Kα radiation (λ = 0.154056 nm). The morphology and structure of the photocatalysts were obtained by field emission scanning electron microscopy (FESEM) at 20.0 kV on a JSM6510A microscope and transmission electron microscopy (TEM) on a JEM-2010 microscope. An X-ray energy-dispersive spectrometer (EDX) was conducted on field emission scanning electron microscopy (FEI Inspect F50). X-ray photoelectron spectroscopy (XPS) was performed on an ESCALAB 250Xi system. The specific surface area of the samples was studied by N_2 adsorption−desorption measurement (Beishide 3H-2000BET-A). UV−vis diffuse reflectance spectra (DRS) were used to investigate the optical properties of the photocatalysts, recorded on a UV-2550 spectrophotometer. The photoluminescence (PL) emission spectra were performed on a fluorescence spectrophotometer (FLS980). The electrochemical impedance spectroscopy (EIS) was conducted on a CHI 760E electrochemical workstation in a classical three-electrode system using Na_2SO_4 aqueous solution (0.5 mol L^{-1}) as an electrolyte.

4.4. Photocatalytic Experiment. The photocatalytic properties of ZnS, In_2S_3, and $ZnS@In_2S_3$ composites were evaluated by the degradation of EB in aqueous solution under simulated sunlight irradiation. At first, 0.05 g of the synthesized

https://doi.org/10.1021/acsomega.2c05483
ACS Omega 2023, 8, 529−538

photocatalyst was dispersed in 100 mL of EB solution (50 mg L^{-1}) under stirring. Then, the solution was ultrasonically dispersed for 10 min and continuously stirred for 10 min in the dark, which would be beneficial for the complete dispersion of the photocatalyst powder and the achievement of the adsorption−desorption equilibrium between the catalyst and the organic dye molecules. Additionally, a 300 W Xe lamp was employed as the simulated sunlight source. Under magnetic stirring, 1 mL of H_2O_2 (30 wt %) was added to the above solution, and at the same time, the photodegradation reaction was induced by the irradiation of the Xe lamp placed 66 cm away from the reactor. Finally, 1 mL of the solution was taken out at an interval of 10 min, diluted to 6 mL with ultrapure water, and centrifuged to remove the residual sample. The real-time concentration of EB was indicated by a UV−vis absorption spectrometer at 514 nm. The absorbances of the pure dye solution and the mixed solution right after the achievement of the adsorption−desorption equilibrium were also measured.

To further prove the excellent performance and the application potential of the photocatalyst, the photocatalytic activity was also evaluated by the degradation of the EB-RhB mixed dye solution. First, 0.05 g of the photocatalyst was added to 100 mL of the mixed solution containing 50 mL of EB and 50 mL of RhB with an initial concentration of 50 mg L^{-1}. Then, the solution was stirred in the dark for 40 min to ensure the uniform dispersion of the photocatalyst and to reach the adsorption−desorption equilibrium. The rest of the photocatalytic process was the same as the degradation of EB mentioned above. The spectra of EB and RhB during the photocatalytic degradation process were measured by a UV−vis absorption spectrometer from 200 to 800 nm.

■ ASSOCIATED CONTENT

Supporting Information

The Supporting Information is available free of charge at https://pubs.acs.org/doi/10.1021/acsomega.2c05483.

XRD pattern of the ZnS precursor; UV−vis diffuse reflectance spectrum of ZnS@In_2S_3-2; EDX results of ZnS@In_2S_3-2 after the photocatalytic process; and BET specific surface areas of ZnS, In_2S_3, and ZnS@In_2S_3 (PDF)

■ AUTHOR INFORMATION

Corresponding Authors

Xiaohui Guan − *School of Chemical Engineering, Northeast Electric Power University, Jilin 132012, P. R. China;* orcid.org/0000-0003-1490-0766; Email: guanxh@neepu.edu.cn

Liu Yang − *School of Chemical Engineering, Northeast Electric Power University, Jilin 132012, P. R. China*; Email: l.yang@neepu.edu.cn

Guangsheng Wang − *School of Chemistry, Beihang University, Beijing 100191, P. R. China;* orcid.org/0000-0002-2408-9260; Email: wanggsh@buaa.edu.cn

Authors

Jianyi Lu − *School of Chemical Engineering, Northeast Electric Power University, Jilin 132012, P. R. China*

Qianqian Guo − *School of Chemical Engineering, Northeast Electric Power University, Jilin 132012, P. R. China*

Jingyang Chen − *School of Chemical Engineering, Northeast Electric Power University, Jilin 132012, P. R. China*

Kunhan Xie − *School of Chemical Engineering, Northeast Electric Power University, Jilin 132012, P. R. China*

Complete contact information is available at: https://pubs.acs.org/10.1021/acsomega.2c05483

Notes

The authors declare no competing financial interest.

■ ACKNOWLEDGMENTS

The authors acknowledge the funding support from the National Natural Science Foundation of China (51972049), the Project of Jilin Province Development and Reform Commission (2021C040-4), and the Science and Technology Research Project of Jilin Education Department (JJKH20210104KJ).

■ REFERENCES

(1) Chen, M.; Guo, C.; Hou, S.; Lv, J.; Zhang, Y.; Zhang, H.; Xu, J. A Novel Z-Scheme AgBr/P-g-C_3N_4 Heterojunction Photocatalyst: Excellent Photocatalytic Performance and Photocatalytic Mechanism for Ephedrine Degradation. *Appl. Catal., B* **2020**, *266*, No. 118614.

(2) Reli, M.; Ambrožová, N.; Valášková, M.; Edelmannová, M.; Čapek, L.; Schimpf, C.; Motylenko, M.; Rafaja, D.; Kočí, K. Photocatalytic Water Splitting over CeO_2/Fe_2O_3/Ver Photocatalysts. *Energy Convers. Manage.* **2021**, *238*, No. 114156.

(3) Wang, Z.; Srivastava, V.; Wang, S.; Sun, H.; Thangaraj, S. K.; Jänis, J.; Sillanpää, M. UVC-Assisted Photocatalytic Degradation of Carbamazepine by Nd-Doped Sb_2O_3/TiO_2 Photocatalyst. *J. Colloid Interface Sci.* **2020**, *562*, 461−469.

(4) Akhundi, A.; Badiei, A.; Ziarani, G. M.; Habibi-Yangjeh, A.; Muñoz-Batista, M. J.; Luque, R. Graphitic Carbon Nitride-Based Photocatalysts: Toward Efficient Organic Transformation for Value-Added Chemicals Production. *Mol. Catal.* **2020**, *488*, No. 110902.

(5) Zhu, S.; Qian, X.; Lan, D.; Yu, Z.; Wang, X.; Su, W. Accelerating Charge Transfer for Highly Efficient Visible-Light-Driven Photocatalytic H_2 Production: In-Situ Constructing Schottky Junction via Anchoring Ni-P Alloy onto Defect-Rich ZnS. *Appl. Catal., B* **2020**, *269*, No. 118806.

(6) Bang, J.; Das, S.; Yu, E.-J.; Kim, K.; Lim, H.; Kim, S.; Hong, J. W. Controlled Photoinduced Electron Transfer from InP/ZnS Quantum Dots through Cu Doping: A New Prototype for the Visible-Light Photocatalytic Hydrogen Evolution Reaction. *Nano Lett.* **2020**, *20*, 6263−6271.

(7) Zhou, J.; Zhao, J.; Liu, R. Defect Engineering of Zeolite Imidazole Framework Derived ZnS Nanosheets towards Enhanced Visible Light Driven Photocatalytic Hydrogen Production. *Appl. Catal., B* **2020**, *278*, No. 119265.

(8) Gao, F.; Lei, R.; Huang, X.; Yuan, J.; Jiang, C.; Feng, W.; Zhang, L.; Liu, P. In Situ Etching Growth of Defective ZnS Nanosheets Anchored Vertically on Layered-Double-Hydroxide Microflowers for Accelerated Photocatalytic Activity. *Appl. Catal., B* **2021**, *292*, No. 120187.

(9) Hao, Q.; Xie, C.; Huang, Y.; Chen, D.; Liu, Y.; Wei, W.; Ni, B.-J. Accelerated Separation of Photogenerated Charge Carriers and Enhanced Photocatalytic Performance of g-C_3N_4 by Bi_2S_3 Nanoparticles. *Chin. J. Catal.* **2020**, *41*, 249−258.

(10) Miodyńska, M.; Mikolajczyk, A.; Bajorowicz, B.; Zwara, J.; Klimczuk, T.; Lisowski, W.; Trykowski, G.; Pinto, H. P.; Zaleska-Medynska, A. Urchin-like TiO_2 Structures Decorated with Lanthanide-Doped Bi_2S_3 Quantum Dots to Boost Hydrogen Photogeneration Performance. *Appl. Catal., B* **2020**, *272*, No. 118962.

(11) Lian, X.; Zhang, J.; Zhan, Y.; Zhang, Y.; Yang, S.; Chen, Z.; Dong, Y.; Fang, W.; Yi, X. Engineering $BiVO_4$@Bi_2S_3 Heterojunction by Cosharing Bismuth Atoms toward Boosted Photocatalytic Cr(VI) Reduction. *J. Hazard. Mater.* **2021**, *406*, No. 124705.

(12) Xin, X.; Song, Y.; Guo, S.; Zhang, Y.; Wang, B.; Yu, J.; Li, X. In-Situ Growth of High-Content 1T Phase MoS_2 Confined in the CuS Nanoframe for Efficient Photocatalytic Hydrogen Evolution. *Appl. Catal., B* **2020**, *269*, No. 118773.
(13) Wu, Z.; Liu, X.; Yu, C.; Li, F.; Zhou, W.; Wei, L. Construct Interesting CuS/TiO_2 Architectures for Effective Removal of Cr(VI) in Simulated Wastewater via the Strong Synergistic Adsorption and Photocatalytic Process. *Sci. Total Environ.* **2021**, *796*, No. 148941.
(14) Zhou, L.; Dai, S.; Xu, S.; She, Y.; Li, Y.; Leveneur, S.; Qin, Y. Piezoelectric Effect Synergistically Enhances the Performance of Ti_{32}-oxo-Cluster/$BaTiO_3$/CuS p-n Heterojunction Photocatalytic Degradation of Pollutants. *Appl. Catal., B* **2021**, *291*, No. 120019.
(15) Sun, G.; Shi, J.-W.; Mao, S.; Ma, D.; He, C.; Wang, H.; Cheng, Y. Dodecylamine Coordinated Tri-Arm CdS Nanorod Wrapped in Intermittent ZnS Shell for Greatly Improved Photocatalytic H_2 Evolution. *Chem. Eng. J.* **2022**, *429*, No. 132382.
(16) Lei, Y.; Wu, X.; Li, S.; Huang, J.; Ng, K. H.; Lai, Y. Noble-Metal-Free Metallic MoC Combined with CdS for Enhanced Visible-Light-Driven Photocatalytic Hydrogen Evolution. *J. Cleaner Prod.* **2021**, *322*, No. 129018.
(17) Shi, Y.; Lei, X.; Xia, L.; Wu, Q.; Yao, W. Enhanced Photocatalytic Hydrogen Production Activity of CdS Coated with Zn-Anchored Carbon Layer. *Chem. Eng. J.* **2020**, *393*, No. 124751.
(18) Wu, T.; Liu, X.; Liu, Y.; Cheng, M.; Liu, Z.; Zeng, G.; Shao, B.; Liang, Q.; Zhang, W.; He, Q.; Zhang, W. Application of QD-MOF Composites for Photocatalysis: Energy Production and Environmental Remediation. *Coord. Chem. Rev.* **2020**, *403*, No. 213097.
(19) Kong, X.; Liu, X.; Zheng, Y.; Chu, P. K.; Zhang, Y.; Wu, S. Graphitic Carbon Nitride-Based Materials for Photocatalytic Antibacterial Application. *Mater. Sci. Eng., R* **2021**, *145*, No. 100610.
(20) Huang, D.; Yan, X.; Yan, M.; Zeng, G.; Zhou, C.; Wan, J.; Cheng, M.; Xue, W. Graphitic Carbon Nitride-Based Heterojunction Photoactive Nanocomposites: Applications and Mechanism Insight. *ACS Appl. Mater. Interfaces* **2018**, *10*, 21035−21055.
(21) Asadzadeh-Khaneghah, S.; Habibi-Yangjeh, A. G-C_3N_4/Carbon Dot-Based Nanocomposites Serve as Efficacious Photocatalysts for Environmental Purification and Energy Generation: A Review. *J. Cleaner Prod.* **2020**, *276*, No. 124319.
(22) Janani, R.; Sumathi, S.; Gupta, B.; Shaheer, A. R. M.; Ganapathy, S.; Neppolian, B.; Roy, S. C.; Channakrishnappa, R.; Paul, B.; Singh, S. Development of CdTe Quantum Dot Supported $ZnIn_2S_4$ Hierarchical Microflowers for Improved Photocatalytic Activity. *J. Environ. Chem. Eng.* **2022**, *10*, No. 107030.
(23) Haque, F.; Daeneke, T.; Kalantar-zadeh, K.; Ou, J. Z. Two-Dimensional Transition Metal Oxide and Chalcogenide-Based Photocatalysts. *Nano-Micro Lett.* **2018**, *10*, No. 23.
(24) Ge, J.; Zhang, Y.; Heo, Y.-J.; Park, S.-J. Advanced Design and Synthesis of Composite Photocatalysts for the Remediation of Wastewater: A Review. *Catalysts* **2019**, *9*, No. 122.
(25) Yan, T.; Tian, J.; Guan, W.; Qiao, Z.; Li, W.; You, J.; Huang, B. Ultra-Low Loading of Ag_3PO_4 on Hierarchical In_2S_3 Microspheres to Improve the Photocatalytic Performance: The Cocatalytic Effect of Ag and Ag_3PO_4. *Appl. Catal., B* **2017**, *202*, 84−94.
(26) Akhundi, A.; Habibi-Yangjeh, A.; Abitorabi, M.; Rahim Pouran, S. R. Review on Photocatalytic Conversion of Carbon Dioxide to Value-Added Compounds and Renewable Fuels by Graphitic Carbon Nitride-Based Photocatalysts. *Catal. Rev.* **2019**, *61*, 595−628.
(27) Xiao, S.; Dai, W.; Liu, X.; Pan, D.; Zou, H.; Li, G.; Zhang, G.; Su, C.; Zhang, D.; Chen, W.; Li, H. Microwave-Induced Metal Dissolution Synthesis of Core−Shell Copper Nanowires/ZnS for Visible Light Photocatalytic H_2 Evolution. *Adv. Energy Mater.* **2019**, *9*, No. 1900775.
(28) Habibi-Yangjeh, A.; Asadzadeh-Khaneghah, S.; Feizpoor, S.; Rouhi, A. Review on Heterogeneous Photocatalytic Disinfection of Waterborne, Airborne, and Foodborne Viruses: Can We Win against Pathogenic Viruses? *J. Colloid Interface Sci.* **2020**, *580*, 503−514.
(29) Wei, Y.; Yang, N.; Huang, K.; Wan, J.; You, F.; Yu, R.; Feng, S.; Wang, D. Steering Hollow Multishelled Structures in Photocatalysis: Optimizing Surface and Mass Transport. *Adv. Mater.* **2020**, *32*, No. 2002556.
(30) Li, X.-B.; Xin, Z.-K.; Xia, S.-G.; Gao, X.-Y.; Tung, C.-H.; Wu, L.-Z. Semiconductor Nanocrystals for Small Molecule Activation *via* Artificial Photosynthesis. *Chem. Soc. Rev.* **2020**, *49*, 9028−9056.
(31) Gao, F.; Yuan, J.; Huang, X.; Lei, R.; Jiang, C.; Zhuang, J.; Liu, P. Directional Transfer of Photo-Generated Charges Mediated by Cascaded Dual Defects in Ternary Photocatalyst ZnS/ZnO-In_2O_3 with Enhanced Photocatalytic Performance. *Chem. Eng. J.* **2021**, *416*, No. 129159.
(32) Xu, L.; Zeng, J.; Li, Q.; Xia, L.; Luo, X.; Ma, Z.; Peng, B.; Xiong, S. X.; Li, Z.; Wang, L.-L.; Lei, Y. Defect-Engineered 2D/2D HBN/g-C_3N_4 Z-Scheme Heterojunctions with Full Visible-Light Absorption: Efficient Metal-Free Photocatalysts for Hydrogen Evolution. *Appl. Surf. Sci.* **2021**, *547*, No. 149207.
(33) Shi, Z.; Li, H.; Zhang, L.; Cao, Y. Improved Photocatalytic Activity of $LaFeO_3$ with Doping Mn^{3+} Ions and Modifying Pd^{2+} Ions for Photoreduction of CO_2 into CH_4. *J. Power Sources* **2022**, *519*, No. 230738.
(34) Zhang, Q.; Hou, T.; Shen, H.; Guan, C.; Duan, L.; Zhao, X. Optical and Photocatalytic Properties of S Doped BiOCl Nanosheets with Tunable Exposed {0 0 1} Facets and Band Gap. *Appl. Surf. Sci.* **2022**, *600*, No. 154020.
(35) Das, P.; Tantubay, K.; Ghosh, R.; Dam, S.; Baskey, M. Transformation of CuS/ZnS Nanomaterials to an Efficient Visible Light Photocatalyst by 'Photosensitizer' Graphene and the Potential Antimicrobial Activities of the Nanocomposites. *Environ. Sci. Pollut. Res.* **2021**, *28*, 49125−49138.
(36) Ouni, S.; Mohamed, N. B. H.; Chaaben, N.; Bonilla-Petriciolet, A.; Haouari, M. Fast and Effective Catalytic Degradation of an Organic Dye by Eco-Friendly Capped ZnS and Mn-Doped ZnS Nanocrystals. *Environ. Sci. Pollut. Res.* **2022**, *29*, 33474−33494.
(37) Kumar, N.; Verma, S.; Park, J.; Srivastava, V. C.; Naushad, M. Evaluation of Photocatalytic Performances of PEG and PVP Capped Zinc Sulfide Nanoparticles towards Organic Environmental Pollutant in Presence of Sunlight. *Chemosphere* **2022**, *298*, No. 134281.
(38) Zhang, W.; Xiao, X.; Zheng, L.; Wan, C. Fabrication of TiO_2/MoS_2@Zeolite Photocatalyst and Its Photocatalytic Activity for Degradation of Methyl Orange under Visible Light. *Appl. Surf. Sci.* **2015**, *358*, 468−478.
(39) Zheng, X.; Fan, Y.; Peng, H.; Wen, J. S-Defected In_2S_3/ZnS Nanospheres for Enhancing Solar-Light Photocatalytic Capacity. *Colloids Surf., A* **2021**, *627*, No. 127126.
(40) Liu, X.; Zhang, T.; Li, Y.; Zhang, J.; Du, Y.; Yang, Y.; Jiang, Y.; Lin, K. Construction of Core-Shell ZnS@In_2S_3 Rhombic Dodecahedron Z-Scheme Heterojunction Structure: Enhanced Photocatalytic Activity and Mechanism Insight. *Chem. Eng. J.* **2021**, *423*, No. 130138.
(41) Yang, L.; Guan, X.; Wang, G.-S.; Guan, X.-H.; Jia, B. Synthesis of ZnS/CuS Nanospheres Loaded on Reduced Graphene Oxide as High-Performance Photocatalysts under Simulated Sunlight Irradiation. *New J. Chem.* **2017**, *41*, 5732−5744.
(42) Guan, X.-H.; Qu, P.; Guan, X.; Wang, G.-S. Hydrothermal Synthesis of Hierarchical CuS/ZnS Nanocomposites and Their Photocatalytic and Microwave Absorption Properties. *RSC Adv.* **2014**, *4*, 15579−15585.
(43) Guan, X.-H.; Yang, L.; Guan, X.; Wang, G.-S. Synthesis of a Flower-like CuS/ZnS Nanocomposite Decorated on Reduced Graphene Oxide and Its Photocatalytic Performance. *RSC Adv.* **2015**, *5*, 36185−36191.
(44) Rao, V. N.; Ravi, P.; Sathish, M.; Reddy, N. L.; Lee, K.; Sakar, M.; Prathap, P.; Kumari, M.M.; Reddy, K. R.; Nadagouda, M. N.; Aminabhavi, T. M.; Shankar, M. V. Monodispersed Core/Shell Nanospheres of ZnS/NiO with Enhanced H_2 Generation and Quantum Efficiency at Versatile Photocatalytic Conditions. *J. Hazard. Mater.* **2021**, *413*, No. 125359.
(45) Jiang, J.; Wang, G.; Shao, Y.; Wang, J.; Zhou, S.; Su, Y. Step-Scheme ZnO@ZnS Hollow Microspheres for Improved Photocatalytic H_2 Production Performance. *Chin. J. Catal.* **2022**, *43*, 329−338.

https://doi.org/10.1021/acsomega.2c05483
ACS Omega 2023, 8, 529−538

(46) You, J.; Liu, C.; Feng, X.; Lu, B.; Xia, L.; Zhuang, X. In Situ Synthesis of ZnS Nanoparticles onto Cellulose/Chitosan Sponge for Adsorption−Photocatalytic Removal of Congo Red. *Carbohydr. Polym.* **2022**, *288*, No. 119332.
(47) Sun, L.; Liu, X.; Ma, T.; Zheng, L.; Xu, Y.; Guo, X.; Zhang, J. In_2S_3 Nanosheets Anchored on N-Doped Carbon Fibers for Improved Lithium Storage Performances. *Solid State Ionics* **2019**, *329*, 8−14.
(48) Hassan, A.; Liaquat, R.; Iqbal, N.; Ali, G.; Fan, X.; Hu, Z.; Anwar, M.; Ahmad, A. Photo-Electrochemical Water Splitting through Graphene-Based ZnS Composites for H_2 Production. *J. Electroanal. Chem.* **2021**, *889*, No. 115223.

https://doi.org/10.1021/acsomega.2c05483
ACS Omega 2023, 8, 529−538